International Journal of Horticultural Science 2025, 31: 73-87.
https://doi.org/10.31421/ijhs/31/2025/15419

Linking bark anatomy to Eucalyptus Physiological Disorder (EPD) in commercial clones

Picoli, E. A. T.[1], Jacomini, F. A.[1], Ladeira, J. S.[1], Almeida, M. N. F.[2], Vidaurre, G. B.[2], Moulin, J. C.[2], Zauza, E. Â. V.[3], Guimarães, L. M. S.[4], Isaias, R. M. S.[5], Balmant, K. M.[6] & Costa, W. G.[7]

[1]Department of Plant Biology, Avenida Purdue, s/n. Campus Universitário da Universidade Federal de Viçosa, Centro de Ciências Biológicas II, Viçosa, MG, Brazil, CEP 36570 900
[2]Department of Forestry Science and Wood, Federal University of Espírito Santo (UFES), Av. Gov. Lindemberg, 316 - Centro, Jerônimo Monteiro, ES, Brazil, CEP 29550-000
[3]Independent Researcher; Rua Rosa Lotfi Almeida Bueno, n. 229, Vila Nastri II, Itapetininga, SP, Brazil, CEP 18206-390
[4]Suzano S.A. Rua Dr. José Lembo, 1010. Bairro Bela Vista; Itapetininga, SP, Brazil, CEP: 18207-780
[5]Biological Sciences Institute (BCI), Minas Gerais Federal University (UFMG), Av. Pres. Antônio Carlos, 6627, Pampulha, Belo Horizonte, MG, Brazil, CEP 31270-901
[6]Horticultural Science Department, University of Florida (UF), 2550 Hull Rd, Gainesville, FL, USA; ZIP 32611
[7]Department of General Biology, Bioinformatics Laboratory, BIOAGRO, Federal University of Viçosa (UFV), Viçosa, MG, Brazil, CEP 36576-900
Author for correspondence: epicoli@ufv.br

Summary: Abiotic stresses trigger the Eucalyptus Physiological Disorder (EPD) which poses a threat to planted and native stands. This research seeks links between eucalyptus bark histological features and EPD, in which the descriptive bark anatomy and histochemistry are approached. Barks from 5-year eucalyptus trees, from commercial clones of *E. grandis*, *E. urophylla* and its hybrids, were collected at breast height (DBH), and 50% and 75% of the commercial height, and evaluated. The eucalyptus bark consisted of a periderm (or rhytidome) and a secondary phloem with conspicuous solitary sieve tube elements (STE). The outer bark revealed a secondary phloem with collapsed STE, whereas its inner counterpart displayed non-collapsed STEs. A region crowded with calcium oxalate (CaOx) crystals in axial parenchyma, covering the non-collapsed and partially overlapped collapsed secondary phloem, was observed. *Eucalyptus* barks exhibited similar anatomical organization at DBH, 50% and 75% of the commercial height, irrespective of expected EPD phenotype or scores. Notwithstanding, there are qualitative differences that are associated with the proportion of non-collapsed phloem and phloem with crystals, which were higher in the tolerant clones and in trees with score 0. The more resistant clones or samples with lower EPD scores exhibited a higher proportion of the regions of living phloem, phloem with CaOx crystals, and non-collapsed phloem. These results support the hypothesis that an increased proportion of STE collapse will occur concurrently with elevated EPD scores and are the basis for an ongoing histometric approach.

Picoli, E. A. T., Jacomini, F. A., Ladeira, J. S., Almeida, M. N. F., Vidaurre, G. B., Moulin, J. C., Zauza, E. Â. V., Guimarães, L. M. S., Isaias, R. M. S., Balmant, K. M., Costa, W. G. (2025): Linking bark anatomy to Eucalyptus Physiological Disorder (EPD) in commercial clones. International Journal of Horticultural Science 31: 73-87. https://doi.org/10.31421/ijhs/31/2025/15419

Key words: bark anatomy, dieback, EPD, *Eucalyptus*, phloem anatomy, planted forest

Introduction

The total area of planted forests in Brazil reached 9.94 million ha in 2022; 76% of which was established with eucalypts (IBÁ, 2023). The eucalypts, including *Corymbia* and *Eucalyptus*, are representatives of native Australian forests that cope with drought, soils poor in nutrients, and fire. Despite the number of eucalyptus species, estimated at around 800 (ABARES, 2019), only nine species and their hybrids comprise the majority of genotypes utilized in eucalyptus planted forests (Stanturf et al., 2013). Eucalypts are one of the most important trees for wood and forestry-derived products due its adaptability and wood quality (ABARES, 2019; Hua et al., 2022).

Natural and planted eucalyptus forests face tree mortality attributed to abiotic stress (Mueller-Dombois, 1986; Fensham & Holman, 1999; Floyd et al., 2009; Matusick et al., 2012; Walden et al., 2019) despite their expected resilience to abiotic stress. The premature death of eucalyptus trees in native and planted forests in Australia has been credited to the physiological disorder since 1920 (Ciesla & Donaubauer, 1994), whereas in Brazil it was first reported as SPEVRD (Seca de Ponteiros do Eucalipto do Vale do Rio Doce) (Ferreira, 1989). Other designations such as "dieback" (Landsberg, 1985; Fensham & Holman, 1999; Matusick et al., 2012) and Eucalyptus Physiological Disorder (EPD) (Câmara et al., 2018; Rodrigues, 2020) are acknowledged and display similar symptoms and etiology (Mueller-Dombois, 1986; Alfenas et al., 2009; Matusick et al., 2012).

EPD is a complex disorder and may cause production and economic losses (Câmara et al., 2018; Walden et al., 2019; Rodrigues et al., 2022) besides negative effects on wood products (Câmara et al., 2018). The disorder has a significant, although opposing, influence on dendrometry, anatomy, chemistry and other wood properties (Corrêa et al., 2017; Câmara et al., 2018; Andrade-Bueno et al., 2020; Almeida et

al., 2022, Nascimento et al., 2024). EPD symptoms are observed in the bark (Alfenas et al., 2009; Câmara et al., 2018), but phloem tissue is poorly characterized (Sevento et al., 2018; Picoli et al., 2021). The oversight of phloem properties in wood-derived products is attributed to the wide spread belief that increased bark percentage is linked to a negative effect on product quality (Foelkel, 2005). Consequently, breeding programs favor wood properties and traits, and impose a neutral (Miranda & Pereira, 2015; Nickolas et al., 2020) or negative (Wei & Boralho, 2000; Pupin et al., 2017; Paludeto et al., 2020) selection to bark features, regardless of the importance of phloem.

Environmental triggers and stress can modulate cell differentiation (Condé et al., 2020a; Moulin et al., 2022), metabolism (Dias et al., 2017; Caetano-Madeira et al., 2023), and other plant systems (Corrêa et al., 2017; Andrade-Bueno et al., 2020; Picoli et al., 2021). It is expected that phloem has a role in the phenotypic plasticity (Rosell, 2016) contributing to EPD resistance. The objective of this report is to compare descriptive anatomical data from bark and secondary phloem of commercial eucalyptus clones and raise features that may be associated with EPD resistance and support for a quantitative analysis.

Materials and methods

This research is part of an inducted research project in collaboration with Suzano S/A (one of the largest companies producing eucalyptus paper and cellulose in the world) aiming at the anatomical characterization of commercial eucalyptus clones. The experiment was conducted in a commercial area known for the occurrence of Eucalyptus Physiological Disorder (Edival A. V. Zauza; personal information), located in in Mucuri municipality (DMS coordinates -18°05'11.00" S -39°33'2.99" W; DD coordinates -18.08639 -39.55083), in the south of Bahia state, Brazil (***Figure 1A***). The experiment was conducted from 2015 to 2020. The site has a climate characterized as Aw (tropical with dry winter) and presented, between 2017 and 2020, an average air temperature of 24°C, precipitation of 915 mm year^{-1}, and a water deficit (estimate) of 380 mm year^{-1}. The rainfall regime in the experimental area was presented in Almeida et al. (2022). The clones were planted with 3x3 m spacing, and cultural practices adopted in the Suzano S.A. commercial areas.

Thirty commercial genotypes, derived from Suzano's breeding program, were screened from which 9 representative of *E. grandis*, *E. urophylla* and *E. grandis* x *E. urophylla* hybrids clones were selected based on their divergent EPD scores in commercial stands, ranging from tolerant, intermediately tolerant to susceptible (***Table 1***). This classification was based on the occurrence of the disorder in commercial plantations and was provided by Suzano S.A. Representative trees were felled and sampled in each plot and were also evaluated according to the EPD symptoms. Dead trees were discarded for sampling. The EPD score and symptom description (Almeida et al., 2022) are shown in ***Table 2***. The experimental design consisted of four blocks with six plants per plot, for each genetic material. All clones had the same age, and were planted at the same site and period. Three of the 4 original blocks were sampled, while the fourth block was preserved according to the company's directives. To reduce uncontrolled bias, the plants evaluated were conducted in a commercial field with standardized management conditions, at the same site, plant age and the same or equivalent position used for sampling the stem.

Stem cross section discs of 4 cm in thickness from 27 trees were sampled at breast height (DBH), and at the positions of 50 and 75% of the commercial height (***Figures 1B*** to ***1D***). The stem discs were cut down into wedges and packed in 300 ml bottles with 70% ethanol (Distribuidora Jandaia, Jandaia do Sul, Brazil), in the proportion of 10 times the sample volume. In the laboratory, the 70% ethanol solution was renewed, and samples submitted to vacuum solution until sub-sampling and processing. Square to rectangular samples with 4-8 mm sides were dehydrated in an increasing graded ethylic series and embedded in methacrylate historesin (Leica, Nussloch, Germany) according to the manufacturer's recommendations, with adaptations. The imbibition period was extended to at least 8 weeks, and the historesin renewed three times. During this process, the samples were subjected to vacuum and maintained at 8ºC. The samples were oriented according to different sectioning plans (***Figures 1E*** and ***1F***), and consisted of bark, cambium and a fragment of the secondary xylem, except for tangential sections that consisted only of periderm or phloem tissues. The sections of 10 µm thickness were obtained in a rotary microtome (Leica, Spencer model) and were used for the descriptive anatomical analysis. The slides of, at least, 81 samples (27 genotypes x 3 positions) in the three section planes were evaluated for anatomy descriptive analysis.

The sections were stained with toluidine blue (O'Brien et al., 1964) and mounted on glass slides with synthetic resin Permount (Fisher, Fair Lawn, USA). Histochemical analyses were carried out using Lugol's reagent for detection of starch (Johansen, 1940), Xylidine Ponceau (XP) for detection of total proteins (Vidal, 1977), Sudan Black (Lison, 1960), and Phloroglucinol, for lignin (Jensen, 1962). Bark tissue macerate was obtained maintaining samples in a 1:1 (v:v) glacial acetic acid (Merk, Darmstadt, Germany) and hydrogen peroxide (Merk, Darmstadt, Germany) for 2-3 days at 60 ºC. The macerate solution was filtered, the samples were washed in running water and stained with Astra blue. Bark descriptive traits followed IAWA list of microscopic bark features (Angyalossy et al., 2016).

Images (anatomical/structural and histochemical analysis) were observed and documented in a photomicroscope (AX70 TRF, Olympus Optical, Tokyo, Japan) with the U-PHOTO system connected to a digital camera (AxionCam Carl Zeiss, Gena, Germany).

Image Pro-Plus® software (version 4.5, Media Cybernetics, Silver Spring, USA) was used to measure lumen and cell wall thickness of the fibers of macerates of samples of the eucalyptus clones.

Results

General description of eucalyptus bark anatomy

Eucalyptus bark samples from different accesses (*E. grandis*, *E. urophylla*, and the urograndis hybrid), expected EPD phenotype (***Table 1***), stem position (DBH, 50% and 75% of the commercial height), and trees with contrasting scores (score "0" or score ≥ "1") exhibited similar histological organization of bark and phloem tissues (***Figure 2***). Although, our focus on descriptive anatomy analysis, macroscopic pictures of eucalyptus stem samples and bark is available in Supplemental ***Figure 1***.

Table 1. Relation eucalyptus clone/sample with the respective phenotypes according historical data of the EPD occurrence in commercial fields and species/pedigree. (Adapted from Nascimento et al., 2024).

Clone - sample	Phenotype (Classification according the company records in commercial fields)	EPD score of the sampled trees	Pedigree
E1 - 1	tolerant	0	*E. urophylla*
E1 - 2	tolerant	0	*E. urophylla*
E1 - 3	tolerant	0	*E. urophylla*
E2 - 4	tolerant	0	*E. urophylla*
E2 - 5	tolerant	0	*E. urophylla*
E2 - 6	tolerant	0	*E. urophylla*
E3 - 7	tolerant	0	*E. grandis* x *E. urophylla*
E3 - 8	tolerant	1	*E. grandis* x *E. urophylla*
E3 - 9	tolerant	1	*E. grandis* x *E. urophylla*
E4- 10	semi-tolerant	0	*E. grandis*
E4 - 11	semi-tolerant	0	*E. grandis*
E4 - 12	semi-tolerant	1	*E. grandis*
E5 - 13	semi-tolerant	0	*E. grandis* x *E. urophylla*
E5 - 14	semi-tolerant	0	*E. grandis* x *E. urophylla*
E5 - 15	semi-tolerant	0	*E. grandis* x *E. urophylla*
E6 - 16	semi-tolerant	0	*E. grandis* x *E. urophylla*
E6 - 17	semi-tolerant	0	*E. grandis* x *E. urophylla*
E6 - 18	semi-tolerant	0	*E. grandis* x *E. urophylla*
E7 - 19	mod-susceptible	1	*E. grandis*
E7 - 20	mod-susceptible	1	*E. grandis*
E7 - 21	mod-susceptible	0	*E. grandis*
E8 - 22	susceptible	2	*E. urophylla*
E8 - 23	susceptible	1	*E. urophylla*
E8 - 24	susceptible	1	*E. urophylla*
E9 - 25	susceptible	3	*E. grandis*
E9 - 26	susceptible	3	*E. grandis*
E9 - 27	susceptible	3	*E. grandis*

Table 2. Symptoms used for the evaluations (scores) of eucalyptus clones in the commercial areas and in the experiment of the scores of Eucalyptus Physiological Disorder (EPD) (According Almeida et al., 2022).

EPD score	Symptom
Level 0	asymptomatic plants
Level 1	depressed surface lesion, cracking and slight detachment of the bark ("scaling"), randomly distributed on the trunk or branches
Level 2	drying of the basal third leaves of the crown, cracking of the bark and swelling at specific points on the stem or randomly distributed along the main stem or branches
Level 3	dieback, bifurcation of the main trunk, sprouting, formation of corky bark, release of bark (exophylactic periderm) and edema (callosity or rough appearance) on the leaves
Level 4	drying canopy and plant death

There are four defined regions in the eucalyptus bark. The first and outer, comprises the periderm/rhytidome. Adjacent to the periderm, outer part of the eucalyptus bark, is a subsequent and disorganized phloem tissue without calcium oxalate crystals (CaOx). This disorganized phloem region overlaps with a third region of collapsed phloem that retains CaOx crystals and, a more internal phloem with non-collapsed STE region crowded with CaOx crystals. The fourth and inner regions, closest to the cambium, exhibits organized phloem cells and non-collapsed solitary STE (***Figures 2A*** and ***2B***). The STE is often accompanied by one companion cell (data not shown) and associated with other axial parenchyma cells. The difference between the companion cell and axial parenchyma is not always clear. These cell types are distributed in tangential bands alternating with tangential bands of rounded to polygonal fibers. The axial parenchyma constitutes the background of the secondary phloem (***Figure 2A***), surrounding STEs, and spaced by rows of fibers. Sieve tube elements are solitary and phloem sclerenchyma is composed only by fibers in tangential bands, and phloem elements nonstoried (***Figure 2A***). Rhytidome is frequently preserved (***Figure 2C***) or may be absent, where at least one periderm is observed (***Figures 2D*** and ***E***), being observed in stem cross sections from DBH to 75% of commercial height, of plants of the same age. The phellem is observed with alternating bands of thin-walled and thick-walled cells (***Figures 2A, 2D*** and ***2E***).

Rhytidome is composed of one or successive developed periderms with a concentric arrangement, although sample processing might have teared outer periderm layers. The rhytidome originates from the several rounds of phellogen formation derived from outer phloem cells in *E grandis*, *E urophylla* and urograndis stems, independent of tree height. The outer rhytidome cells are collapsed compared to its inner counterpart (***Figures 2A*** and ***2C***). There was an average of 1.7, 1.8 and 3.3 periderm layers from 75%, 50% commercial height, and DBH respectively. Hence the rhytidome was better

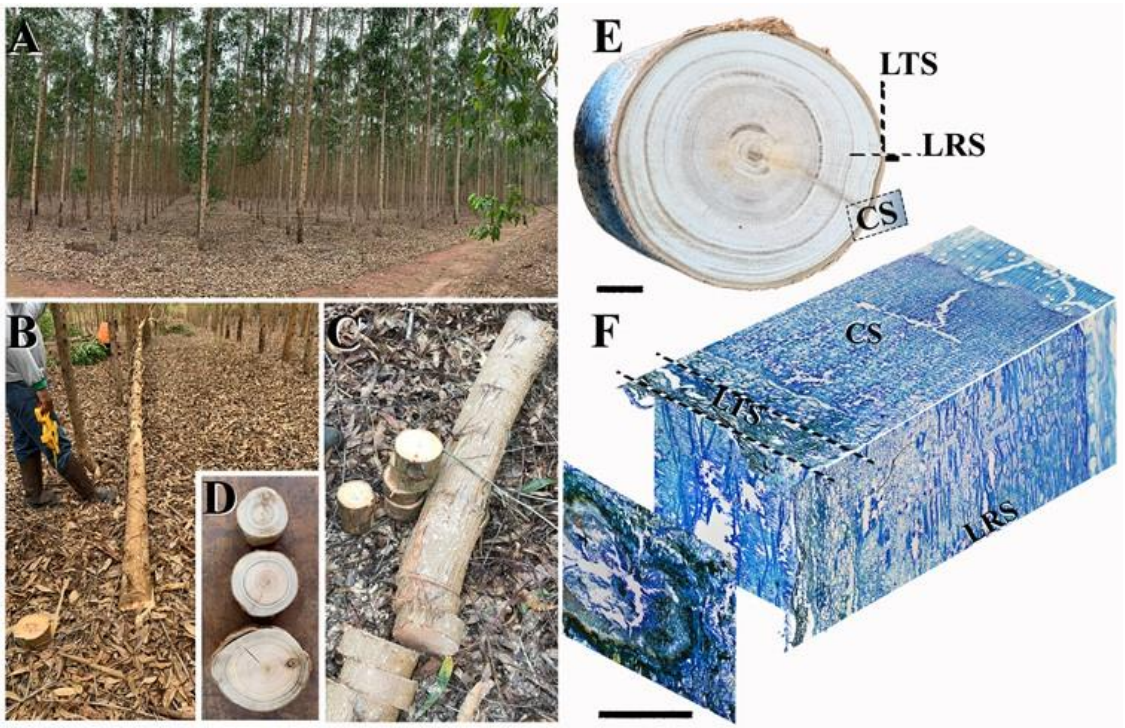

Figure 1. Eucalyptus plantation, Suzano's experimental field, stem disks sampling, and orientation and view of the sections. A – panoramic view of the commercial field where the experiment was conducted; B – felled eucalyptus tree; C – stem disks sampling; D – sampled stem disks at DBH, 50% and 75% of commercial plant height (bottom – up); E – stem disk illustrating the position and orientation for bark sections (sample 16, *E. grandis* x *E. urophylla*); F – histological sections in different orientation, transversal, longitudinal tangential and longitudinal radial, xylem (greenish blue), secondary phloem and periderm tissues (sample 21, *E. grandis*). Bar – E = 2 cm and F = 1000 µm. CS, cross section; LRS, longitudinal radial section; LTS, longitudinal tangential section.

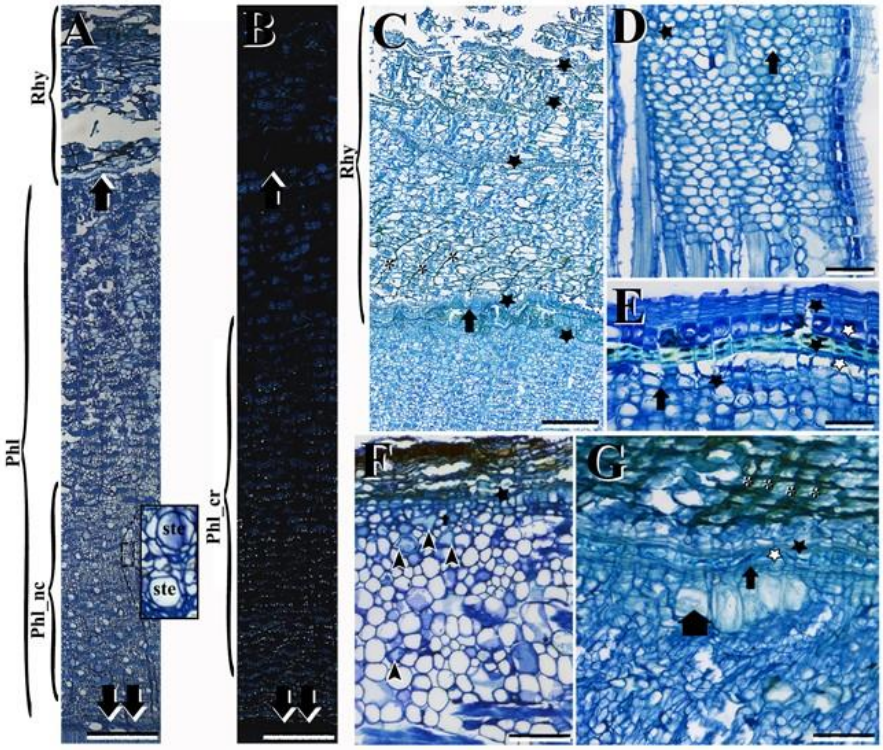

Figure 2. Details of the cross and longitudinal sections of eucalyptus bark. A – cross section of eucalyptus bark, observe the rhytidome (Rhy), secondary phloem tissues (Phl) and non-collapsed secondary phloem (Phl_nc). The more recently formed phellogen (one black arrow) and cambium region (two black arrows) are highlighted (sample 16, *E. grandis* x *E. urophylla*), detail of sieve tube elements (ste) (transversal section); B – cross section of eucalyptus bark under polarized light, observe the domain of live phloem cells with CaOx (Phl_cr). The more recently formed phellogen (one black arrow) and cambium region (two black arrows) (sample 16, *E. grandis* x *E. urophylla*) (transversal section); C – rhytidome (Rhy), with evident layers of older phellogen (stars) and recently isolated phloem rays (asterisks) (sample 4, *E. urophylla*) (transversal section); D – bark longitudinal section with absent rhytidome, details of merged parenchyma ray, phellogen (arrow), and phellem (black star) (sample 4, *E. urophylla*) (radial section); E – bark section with absent rhytidome, details of alternate thick cell wall (black star) and thin cell wall phellem cells (white star), and phellogen (arrow) (sample 4, *E. urophylla*) (radial section); F – outer bark region with disorganized parenchyma and parenchyma with lignified cell walls (arrow heads), phelloderm (arrow), and phellogen (star) (sample 4, *E. urophylla*) (radial section); and G – detail of outer bark, thin-walled phellem cells (white stars), thick-walled phellem cells (black star), phellogen (long arrow), outer phloem disorganized and thin-walled large parenchyma cells (larger arrow), and recently isolated and phenolized phloem rays (asterisks) (sample 8, *E. grandis* x *E. urophylla*) (radial section). Bar – A = 1000 µm, B = 1000 µm, C = 1000 µm, D = 100 µm, E = 50 µm, F = 100 µm, and G = 100 µm.

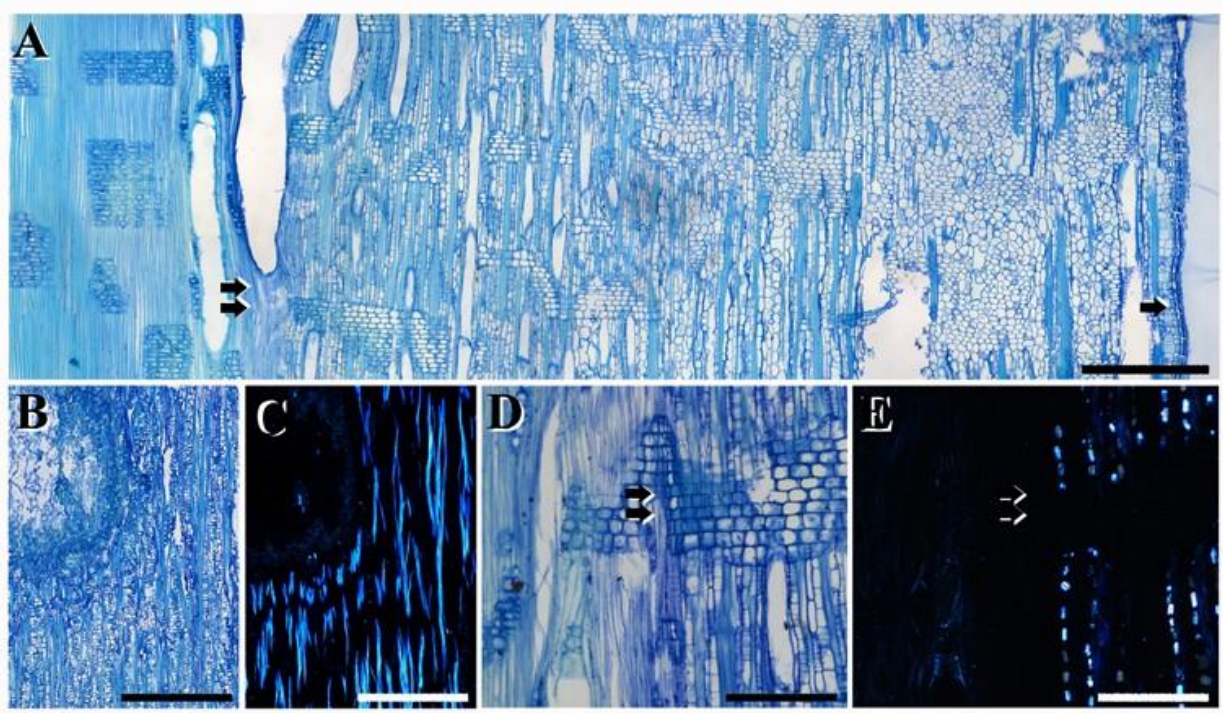

Figure 3. Details of the cross and longitudinal radial sections of outer bark/secondary phloem. A – longitudinal radial section of eucalyptus bark. The more recently formed phellogen (one black arrow) and cambium (two black arrows) (radial section); B – tangential section with the phloem-periderm transition; C – longitudinal tangential section of the same region under the polarized light highlighting outer phloem fibers; D – radial section of a stem region near the cambium, on the left xylem tissue and on the right secondary phloem tissue are observed. Cambial initials (two black arrows) are highlighted; E – radial section with the same region under polarized light, highlighting CaOx crystals (bright inclusions) and cambial initials region (two black arrows); A = 1000 µm, B = 1000 µm, C = 1000 µm, F = 400 µm, and G = 400 µm.

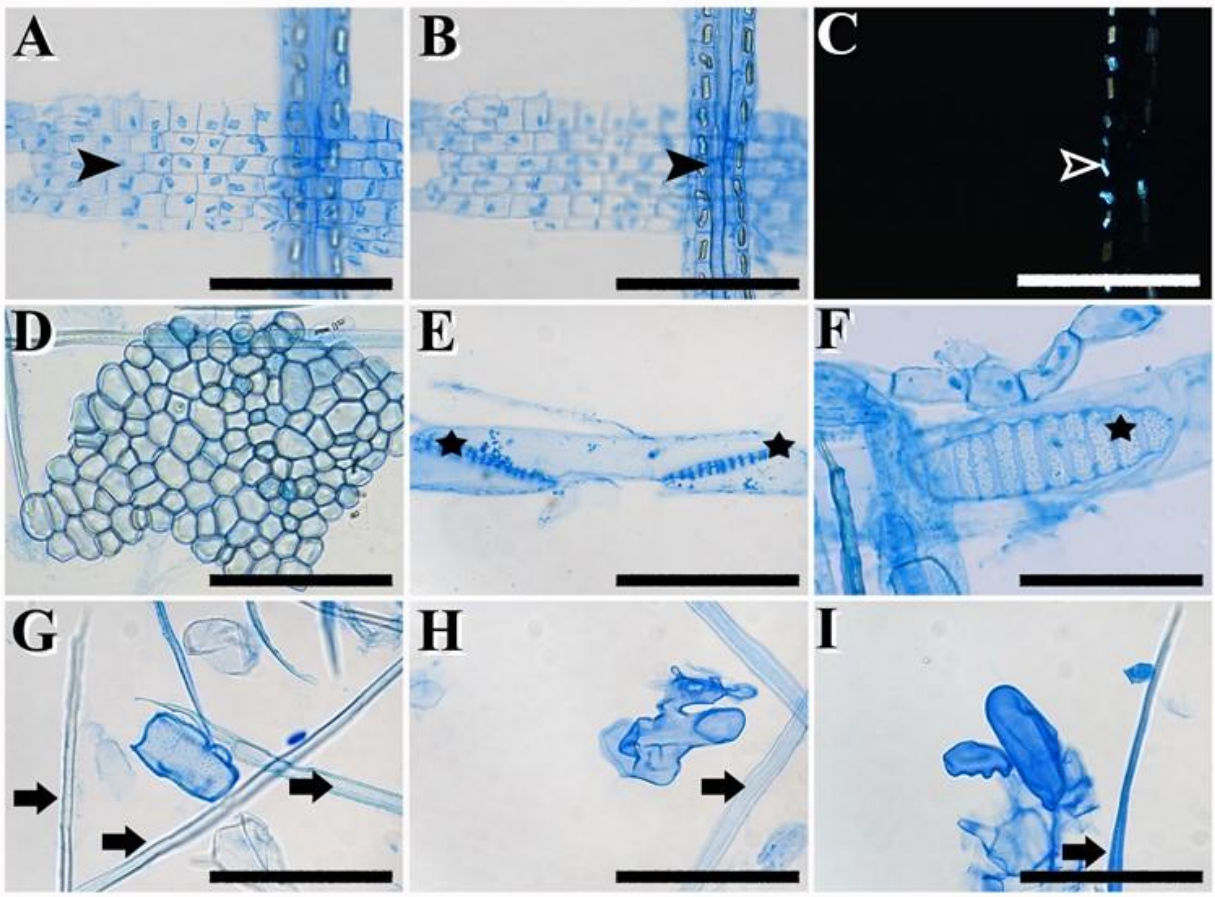

Figure 4. Bark/secondary phloem macerate. A – square shaped radial parenchyma cells (arrow head); B – axial parenchyma cells highlighting Ca oxalate crystals (arrow head); C – axial parenchyma cells with CaOx crystals under polarized light (white/black arrow head); D – putative periderm cell aggregates; E – STE and contacting sieve plates (stars); F – frontal view of a compound sieve plate (star); isolated phloem fibers (arrows) and sclerified parenchyma cell; G – sclerified parenchyma cell and fiber cell (arrow); H – sclerified parenchyma cell with intrusive growth and fiber cell (arrow); and I – sclerified parenchyma cell with less conspicuous intrusive growth and fiber cell (arrow). Bar – A, B, C, and D = 500 µm, E = 200 µm, F = 100 µm, G, H and I = 500 µm.

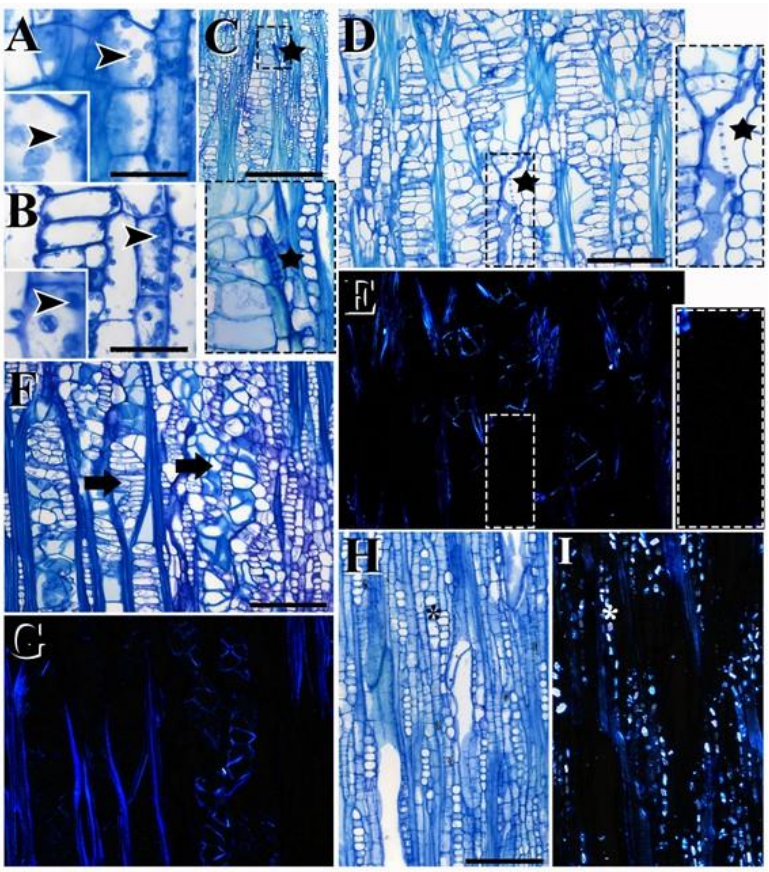

Figure 5. Details of periderm and secondary phloem structure in longitudinal tangential sections. A – detail of plastids (arrow heads) in outer phloem axial/ray parenchyma cells closer to the periderm The small box on the downside left is an ampliation of the plastid; square shaped radial parenchyma cells (arrow head) (tangential section); B – detail of parenchyma cells closer to the periderm with plastids (arrow heads) with denser content (tangential section); C – section of outer phloem with enlarge parenchyma cells and a collapsed STE, hatched square is amplified in the detail. The black star marks the sieve plate, (tangential section); D – section of outer secondary phloem of *E. urophylla* with enlarged parenchyma cells and a partially collapsed STE, hatched box is amplified with a detail of the sieve plate (black stars) (tangential section); E – section of the same section of outer secondary phloem of *E. urophylla* with polarized light. Parenchyma and STE are not evident whereas only fiber cells are evident (tangential section); F – section of outer secondary phloem of *E. grandis* with prominent tangentially enlarged parenchyma cells and parenchyma cells with a thick lignified cell wall (black arrows) (tangential section); G – the same section of outer secondary phloem *E. grandis* observed in polarized light, thick and lignified cell walls are in evidence (tangential section); H – section of inner secondary phloem with preserved parenchyma rays (asterisk). See also the lumen of the SCEs (tangential section); and I – section of the same inner secondary phloem under polarized light (tangential section). The Ca oxalate crystals are evident in axial phloem axial parenchyma cells. Bar – A = 50 μm, B = 50 μm, C = 1000 μm, D = 200 μm, E = 200 μm, F = 400 μm, G = 400 μm, H = 200 μm, and I = 200 μm.

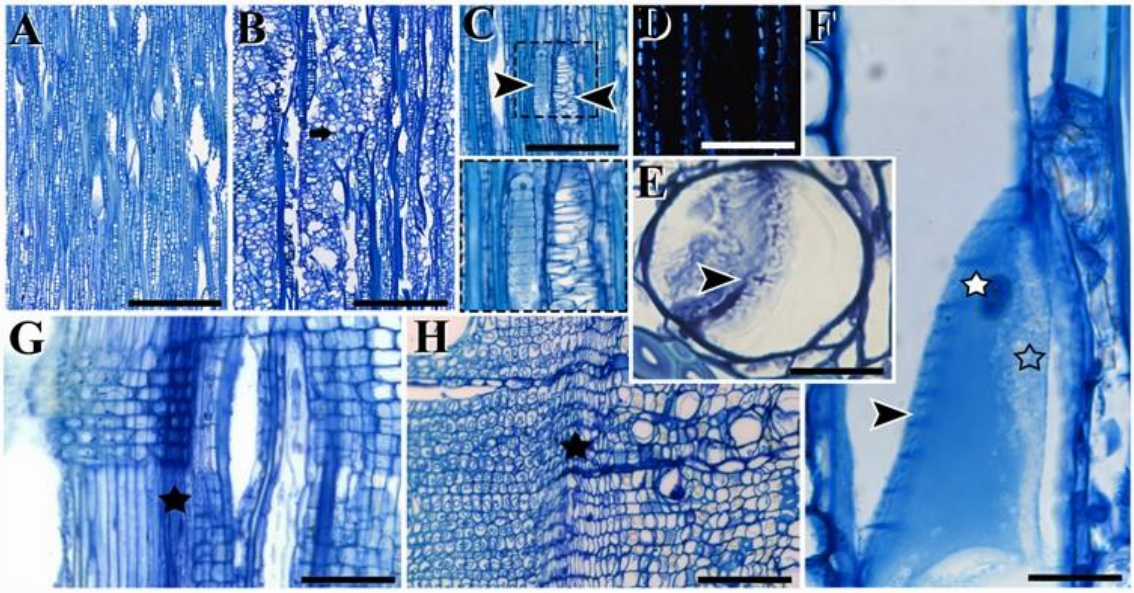

Figure 6. Details of different sections of the eucalyptus sections and sieve plate. A – section of non-collapsed phloem domain (tangential section); B – section of collapsed phloem domain (tangential section); C – preserved and disrupted sieve plate (arrowheads). The detail is an amplification of the sieve plates (radial section); D – the same region of the preserved and disrupted sieve plate (arrowheads) observed under the polarized light (radial section); E – cross section of the sieve plate (arrowhead) (transversal section); F – longitudinal view of a sieve plate (arrowhead), and details of the P-type plastid (white star) and small S-type plastids (star without filling) (tangential section); G – longitudinal radial section highlighting the cambium (black star) (radial section); H – cross section highlighting the cambium (black star). (transversal section). Bar – A = 400 μm, B = 500 μm, C and D = 100 μm, E and F = 50 μm, G = 100 μm, and H = 500 μm.

observed at DBH. Despite statistical test was not applied and due expected bias attributed to natural periderm peel or during sample processing is expected, an average of 4.7 periderms were recorded for the moderate susceptible samples, and 2.6, 1.9 and 1.9 periderm layers for the tolerant, semi-tolerant and susceptible clones, respectively. Similar number of periderms in the rhytidome were observed for *E. urophylla* (2.5), *E. grandis* (2.1) and their hybrid (2.8).

Outer periderm layers showed collapsed phloem cells making it not possible to count the cell layers, although non-collapsed parenchyma and STE cells, closer to the inner periderm was observed less frequently. It was feasible to count the number of fiber groups between two consecutive periderms, what is an approach of the amount of phloem tissue eliminated with the successive periderm formation. Average number of fiber layers were observed for the 75%, 50% commercial heigh and *E. urophylla* (3.5), *E. grandis* (4.8) and their hybrid (4.6) barks. Although bias is expected due natural causes or sample processing, tolerant clones had an average of 2.6 fiber cell groups, followed by 5.0 in the semi tolerant, 6.4 in the moderately susceptible and 6.6 in the susceptible eucalyptus clones. The susceptible clones seem to be more prompt to eliminate phloem cell layers with the newly formed periderms. The inner and more recently differentiated periderm is continuous throughout the evaluated samples and shows an average of 5 phellem, 1 to 5 phelloderm, and 2 phellogen cell layers, in all stem positions and clones evaluated. Phellem is stratified displaying alternating bands of thin walled and thick, lignified cell walls (2 to 3 cells per layer), or without thickened walls (2 to 7 cells per layer) (***Figures 2C to 2E***).

Phelloderm cells are rectangular, and phellem has alternating cell layers with thick and thin walls. Phellogen cells are a little smaller than phellem and phelloderm, and phellogen and phelloderm may have a dense content in cytoplasm. In the rhytidome, these phellem cells contrast with fiber cells that display round to prismatic shapes in cross sections (***Figures 2A*** and ***2C***). Phellogen is restricted to 1 to 2 cell layers, whereas phelloderm account for 1 to 5 cell layers. Merged parenchyma rays, or group of collapsed secondary phloem cells, may be observed in the boundary of inner and newly formed periderm (***Figure 2D***) as well as disorganized parenchyma cells (***Figures 2F*** and ***G***). Sporadically, enlarged parenchyma cells are observed in the limit of phelloderm and phloem (***Figure 2G***). Phenolization is common in rhytidome (***Figure 2G***) where irregular groups or cells in a row displays a greenish color associated with the presence of phenolics. The periderm and phellogen (***Figures 3B*** and ***3C***) and cambial cells (***Figure 3D*** and ***3E***) lack CaOx crystals.

The different cell types of eucalyptus secondary phloem are depicted in ***Figures 2A, 2B, 4A to 4F,*** and ***5A to 5I***. Plastids are observed in phelloderm and outer phloem parenchyma cells (***Figures 5A*** and ***5B***). Growth rings are not observed in eucalyptus secondary phloem. The inner and outer phloem, next to the cambium and the phellogen, respectively, have a different organization (***Figures 2A, 2B,*** and ***3A***). The outer phloem has less organized and enlarged parenchyma cells (***Figures 2F, 2G, 3A***) or lignified wall thickenings (***Figure 2F***, ***4G, 4H*** and ***4I***). These cells are identified as sclereids that, although less frequent, may be formed in the course of phloem dilatation. This characterizes a dilatation in the rays by cell expansion, although axial parenchyma expansion and collapse is observed. The course of rays is undulated, and parenchyma cells from the inner phloem are organized and less expanded (***Figures 2A, 3A, 3D, 4A*** and ***4B***). The diming of CaOx crystals in polarized light is concomitant with the increasing collapse of STE, disorganization of phloem cells (***Figures 2A, 2B, 5C to 5I***), and the differentiation of phellogen initials.

In the outer phloem, axial parenchyma undergoes, mainly, a tangential expansion. Although possible, there was not observed signs of cell divisions. Axial parenchyma cells also undergo radial expansion, but less frequently and conspicuous than ray parenchyma. The ray parenchyma in the outer phloem may occasionally exhibit one round of cell division (***Figures 5C, 5D,*** and ***5F***). Outer axial parenchyma cells enlarge, concomitantly with STE collapse, and an apparent loss of CaOx crystals (***Figures 5C to 5I***). The CaOx are observed to fade in the outer layers of axial parenchyma and also seem to be smaller in size compared to the crystals examined in inner secondary phloem layers. The expansion of ray parenchyma cells may occur concomitantly with axial parenchyma cell wall thickening and lignification in longitudinal tangential sections (***Figures 5D*** and ***5F***). Sclerification of outer parenchyma cells is observed in the non-conducting (collapsed) phloem, although there is little cell wall thickening. The lack of crystals in the outer secondary phloem of *E. grandis* and *E. urophylla* is evidenced (***Figures 5D, 5E, 5F*** and ***5G***).

The boundary of the collapsed and non-collapsed phloem is determined by examining the collapse of the STE and expansion of parenchyma cell in the outer phloem. Similarly, the phloem region containing CaOx crystals is, as delineated by their presence, detected under polarized light (***Figures 2A*** and ***2B***). Although both are birefringent, CaOx crystals are brighter and fibers assumed a bluish color (***Figures 5G*** and ***5I***). The STE is occasionally observed in the collapsed region and identified based on the presence of collapsed or partially collapsed sieve plates (***Figures 5C, 5D,*** and ***5F***). In the non-collapsed phloem, parenchyma cells are thin-walled (Figures 4A and 4B), while in the collapsed region they may undergo cell wall thickening and lignification (***Figures 4G, 4H*** and ***4I***) or expand and grow, being reshaped to a roundish form (***Figures 5C to 5G***). The lignified cells are roundish-rectangular (***Figures 4G*** and ***4I***) to irregular (***Figure 4H***), and presenting projections that should fit in small intercellular spaces (***Figures 4G, 4H,*** and ***4I***).

Parenchyma rays are homogenous, with procumbent cells; and uniseriate (***Figure 5H***), ranging from 5 to 16 cells in height, independently from stem position, species, or EPD phenotype. Tangential sections of inner secondary phloem exhibit prismatic CaOx in phloem axial parenchyma (***Figures 4H*** and ***4I***). The presence of calcium oxalate crystals diminishes gradually from the middle towards the outer layers of the phloem, as depicted in ***Figures 2B, 3C,*** and ***3E***. Notably, these crystals are only found in the phloem axial parenchyma, and are absent in ray parenchyma cells, as well as in recently formed xylem axial parenchyma (***Figure 2E***), and the outer layers of the phloem, as seen in ***Figures 2G, 5E,*** and ***5G***. The axial parenchyma consists of rows of square to rectangular cells, orientated in the stem base-up direction. The outer axial parenchyma layers lack CaOx crystals, may have thicker and lignified cell walls (***Figures 5 D to 5G***), and vary in size about doubling the diameter of the inner layers (***Figures 5H*** and ***5I***). These cells often contain CaOx crystals (***Figures 2B, 3E, 4A, 4B, 4C,*** and ***5I***), adjoined to STE and fibers in inner phloem (***Figures 4B, 4C, 5H*** and ***5I***). Axial parenchyma and fibers are aligned in tangential bands interrupted by radial rays and may be displaced due to the differentiation of other rounding phloem cells (***Figures 2A, 3A, 5C to 5I***). There is a wide variation, but 1 to 3 cell layers of axial parenchyma in the

radial (outward), and 4 to 7 cell layers in the tangential direction, are frequently observed.

Phloem fibers are characterized by thick secondary walls (***Figures 4G to 4I***). Initial estimates of fiber average 18 ± 3.5 µm in diameter and 892.6 ±334.8 µm in length. Fiber lumen showed an average of 7.3 ± 4.6 µm and a coefficient of variation of 62.4 %, higher than observed for average diameter and length, 19.3 and 26.4 %, respectively. Despite a great amplitude in dimension, the lumen diameter is associated with different differentiation stages or accountable differences in overall fiber diameter and cell wall thickness.

Dilatation was observed in both axial parenchyma and phloem rays, where axial parenchyma undergoes cell expansion and rays being slightly dilated resulting in the increase in bark circumference and adjustment of phloem tissues to the xylem secondary growth (***Figures 5H*** and ***5I***) and become increasingly disorganized toward the outer phloem due to parenchyma cell expansion and STE collapse (***Figures 5C, 5D*** and ***5F***). Phloem fibers are 10 fiber-cell layers long and 1 layer of fiber cell layers thick (radially). The number of parenchyma and fiber cell layers varied. Fibers occurred in rows with a variable number of cells although 2 and 3 rows of fibers were observed in the radial direction and were commonly observed between rays. No trend of the number of axial parenchyma or fibers cell layers was observed among the clones and stem positions evaluated.

The conspicuous diameter, form, and the presence of the sieve plate allowed the identification of STE in cross sections (***Figures 2A to 2D***). The non-collapsed STE is also observed in the radial and tangential sections (***Figures 3A*** and ***5H***). All genotypes and EPD score samples presented collapsed and non-collapsed scalariform sieve plates (***Figures 4E*** and ***4F***). A collapsed STE in *E. grandis* outer phloem (***Figure 5C***) and a partially collapsed sieve plate in *E. urophylla* phloem are illustrated (***Figure 5D***). All genotypes exhibit inclined compound sieve plates (***Figures 4E*** and ***4F***), mostly with >20 sieve areas, ranging from 24 to 45.

Observations reveal a collapse of sieve tube elements (STE) progress, from the inner to the outer and less organized phloem (***Figures 6A*** and ***6B***) across samples from all clones and stem positions. Additionally, disrupted sieve plates are evident (***Figures 6C*** and ***6D***). Non-collapsed STE have a dense cytoplasm residue precipitated with different plastids (***Figures 6E*** and ***6F***), and are observed near the cambium (***Figures 6G*** and ***6H***). Phloem radial initials are smaller and contain a dense content, as do rays closer to cambial initials (***Figures 6G*** and ***6H***). Independently from position, species and EPD scores, vascular cambium ranged from 5 to 16 cells.

Differences among EPD tolerant/susceptible clones, and trees with different EPD scores

Intact STE are circumscribed to the newly formed phloem close to cambial initials (***Figures 2A, 3A, 6G, 6H***). Additionally, they are more preserved in EPD-tolerant genotypes and in plants without disorder symptoms. The regions containing non-collapsed STE and phloem cells with crystal formations are broader in tolerant trees and within the same clone but with varying EPD scores, as illustrated in ***Figure 7***. These regions and differences are represented by samples of the same clone (***E3***, ***Table 1***) with different scores, "zero" (0) (***Figures 7A*** and ***7C***) and "one" (1) (***Figures 7B, 7D***). The limits of the non-collapsed regions and phloem with crystals used for the characterization are highlighted in ***Figures 7E to 7H***.

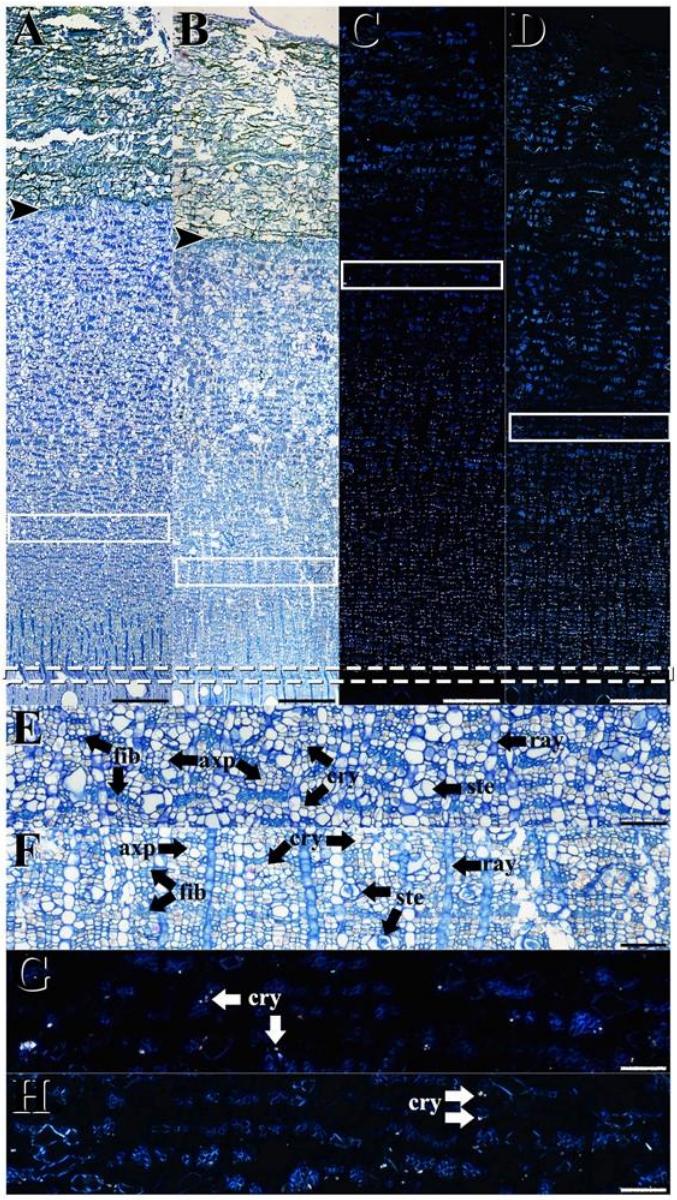

Figure 7. Bark cross sections of the same clone (E3) with different EPD scores all transversal sections. The cambium at the base of sections (rectangle with dashed line limits) and the more recently formed periderm (arrowhead) are evidenced. A – bark from a EPD score 0 (zero), the limit from the collapsed to the non-collapsed phloem region is highlighted; B – bark from a EPD score 1 (one), the limit from the collapsed to the non-collapsed phloem region is highlighted; C – bark from a EPD score 0 (zero), the limit from the phloem region with and without CaOx crystals is highlighted; D – bark from a EPD score 1 (one), the limit from the phloem region with and without CaOx crystals is highlighted; E – detail of the limit of the collapsed to the non-collapsed phloem region , EPD score 0 (zero), F – detail of the limit of the collapsed to the non-collapsed phloem region , EPD score 1 (one); G – detail of the limit of the phloem with and without CaOx crystals, EPD score 0 (zero), H – detail of the limit of the phloem with and without CaOx crystals , EPD score 1 (one). Bar – A, B, C, and D = 500 µm; E, F, G, and H = 200 µm. fib, fibers; axp, axial parenchyma; cry, CaOx crystals; ray, parenchyma ray; ste, sieve tube element. (images A, C, E, G from sample 7, and B, D, F, H from sample 8, both *E. grandis* x *E. urophylla*).

The region of secondary phloem with non-collapsed STE ranged from ½ to 1/3, ½ to 1/6 and 1/3 to 1/10 for the tolerant, semi-tolerant, and susceptible clones, respectively. The periderm, or rhytidome, was not considered in these estimates as they may have been detached from the bark during processing or by natural causes or as a technique artifact. Some rays with 24-30 cells are observed more frequently in the outer phloem of susceptible clones, and are interpreted as being merged from smaller rays.

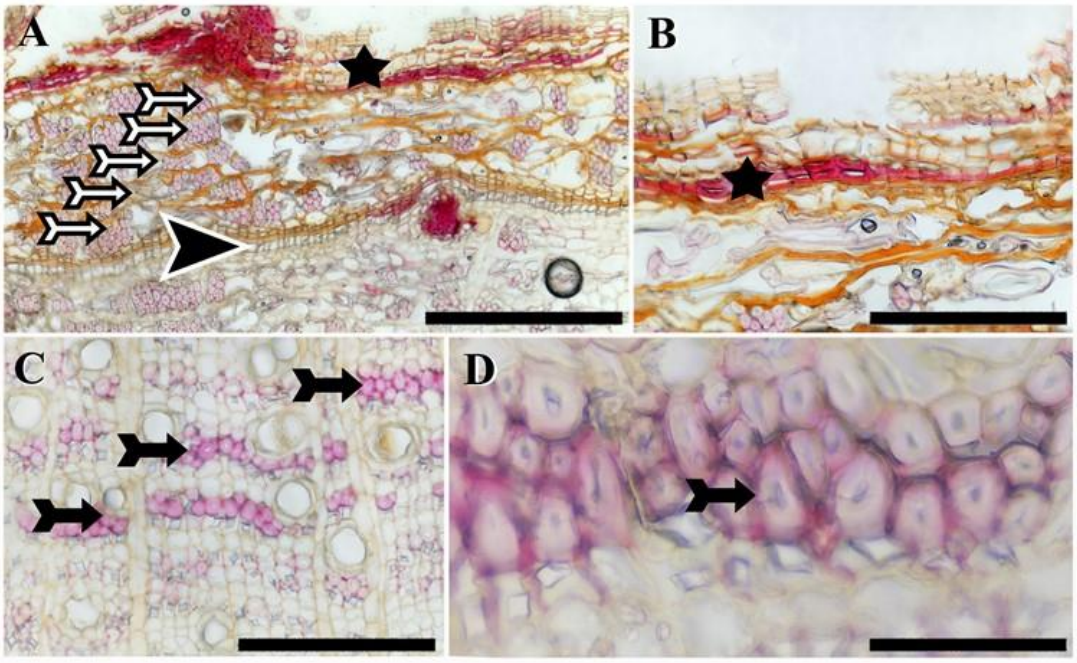

Figure 8. Histochemical reactions for lignin (phloroglucinol) in the periderm and secondary phloem tissues. All transversal sections. A – periderm cross section highlighting collapsed phloem cells, negative for lignin and more preserved fiber cells with thick cell walls with a light positive reaction (redish color) for lignin. The outer phellem cells (black star), layers fibers and other collapsed cells from the secondary phloem (black & white arrows), and the phellogen (white & black arrowhead) are highlighted; B – detail of the outer phellem cells with thick cell walls displaying positive reaction for lignin (black star); C – non-collapsed secondary phloem with fiber cells with a light positive reaction to lignin (black arrows); and D – detail of the fiber cells and cell walls emphasizing a stronger lignification at the outer cell wall (black arrows). Bar – A = 400 µm, B and C = 200 µm, and D = 50 µm. (all images from sample 18, *E. grandis* x *E. urophylla*).

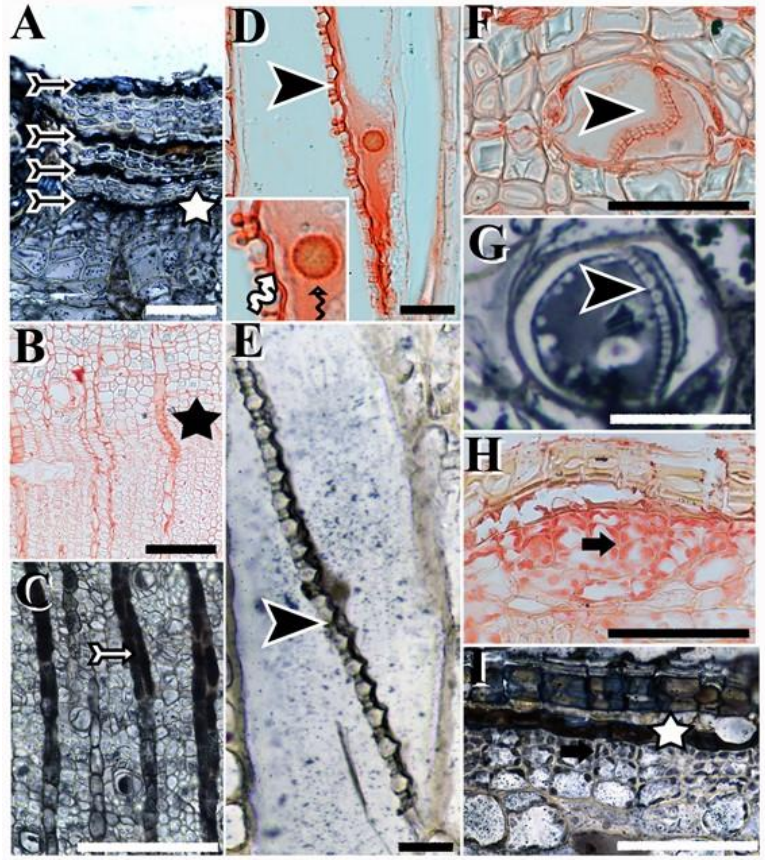

Figure 9. Histochemical reactions for protein (Xylidine Ponceau) and lipids (Sudan Black) in bark tissues. A – strong positive reaction for lipids in the thin cell wall of phellem cells, interspaced with thick cell walls of phellem cells. White star marks the phellogen (transversal section); B – slight positive reaction for protein in radial initials and immediate derived cells (transversal section); C – positive reaction for lipids in secondary phloem radial parenchyma (arrow) in the non-collapsed phloem (transversal section); D – positive protein reaction in STE at the region near the sieve plate. Observe a light precipitation in the cytoplasm and a stronger reaction of a layer in contact with the sieve plate (arrowhead). The detail is an amplification of the P-type plastid (curved black arrow) and positive reaction for the layer in contact with the sieve plate (tangential section); E – positive lipid reaction in STE at the region near the sieve plate (arrowhead) (tangential section); F – Cross section of the sieve plate and light reaction for protein in the cytoplasm near the sieve plate (arrowhead) (transversal section); G – positive reaction for lipids in the cytoplasm close to the sieve plate (black arrowhead) (transversal section); H – positive protein reaction in the plastids in the cells close to the phellogen (black arrows) (transversal section); I – positive reaction for lipids in the phellogen initials (white star) and light positive reaction in the plastids of the phelloderm (black arrow) (transversal section). Bar – A, B, and C = 125 µm, D = 50 µm, E = 25 µm, F, G, H, and I = 125 µm. (all images from sample 7, *E. grandis* x *E. urophylla*).

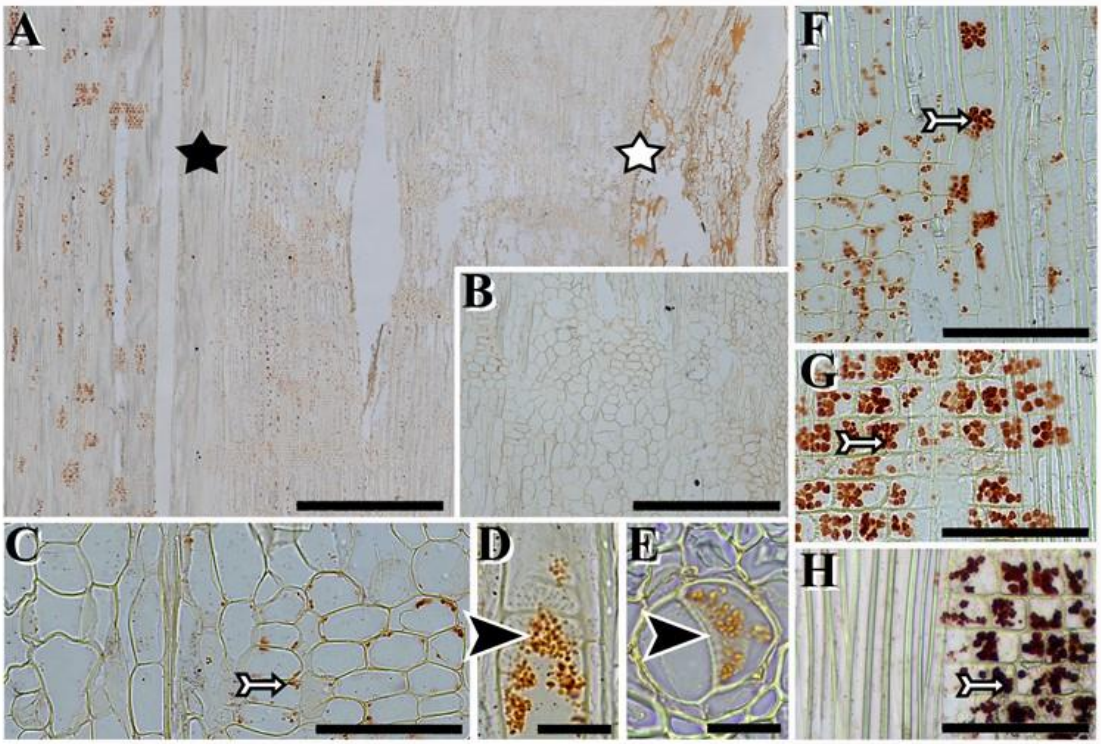

Figure 10. Histochemical reactions for starch (Lugol) in bark and secondary xylem tissues. A – longitudinal radial section with small amyloplasts in axial and radial phloem parenchyma. The cambium (white star) and phellogen (black star) are highlighted (radial section); B – detail of the outer parenchyma cells, close to the phellogen, with no reaction for starch (radial section); C – small plastids testing positive for starch in phloem radial parenchyma cells (white arrow) (radial section); D – longitudinal section of phloem, small plastids testing positive for starch in STE (black arrowhead) (radial section); E – phloem cross section, small plastids testing positive for starch in STE (black arrowhead) (transversal section); F – longitudinal xylem section, light reaction for starch in xylem radial parenchyma cells (white arrow) (radial section); G – longitudinal xylem section, stronger reaction for starch in xylem radial parenchyma cells (white arrow) (radial section); and H – positive reaction for starch in axial and radial phloem parenchyma cells, detail of bigger plastids in axial parenchyma (white arrow) and smaller plastids in radial parenchyma cells (radial section). Bar – A = 1000 µm, B = 400 µm, C = 100 µm, D and E = 25 µm, F, G, and H = 100 µm. (Images A, F, D, E, G from sample 1, E. *urophylla*; images B, C, H from sample 20, *E. grandis*).

Histochemical analysis

The histochemical approach of bark contributed to elucidating the characteristics of the periderm and phloem. The phellem cells with thicker cell walls are strongly lignified (***Figures 8A*** and ***8B***). Several layers of other phloem cells, including parenchyma and STE, which are shed with the formation of the new periderm, tested negative for the presence of lignin (***Figure 8A***). Fibers from the collapsed and non-collapsed phloem have unevenly lignified walls. The middle lamella is more lignified compared to the fiber inner secondary wall layers (***Figures 8C*** and ***8D***). Lipidic substances were detected in the phellem cells (***Figure 9A***).

The dense cytoplasm observed in ray cells, specifically in the non-collapsed phloem near the cambium, is attributed to increased amounts of protein (***Figure 9B***) and lipids (***Figure 9C***) compared to the axial parenchyma cells. A dispersive P-Protein, a proteinaceous residue, and larger, round plastids rich in protein (P-type) inside the STE are illustrated in ***Figure 9D***. Proteins (***Figures 9D*** and ***9F***) and lipids (***Figures 9E*** and ***9G***) are also evidenced in the STE and on the surface of the sieve plates. The plastids in the phelloderm or outer phloem region also exhibited proteins (***Figure 9H***) and lipids (***Figure 9I***).

Starch was detected in the bark samples and xylem tissues. Amyloplasts were noticed in axial and radial parenchyma cells of the secondary phloem and xylem cells (***Figure 10***). Starch is observed in xylem rays (***Figure 10A***) and smaller grains. Yet, absent in the outer and disorganized parenchyma cells (***Figures 10B*** and ***10C***). STE harbor different size plastids. The smaller (S-type) with starch (***Figures 6F, 10D*** and ***10E***) and the bigger (P-type) with protein inclusion (***Figure 9D***). Tolerant eucalyptus exhibited small and slightly increased starch grains in the inner phloem parenchyma (***Figure 10F***) compared to the susceptible clones. Xylem parenchyma rays also have amyloplasts in tolerant and susceptible clones (***Figure 10G*** and ***10H***).

Discussion

Bark represents a considerable amount of eucalyptus stems. It comprises 7.7 to 18.0% or more of the stem, depending on the age and species of the eucalyptus (Ramirez et al., 2009; Almeida et al., 2022). There are morphological differences that can be attributed to different eucalyptus species (Dutkowski & Potts, 1999; Brando et al., 2012; Wesolowski et al., 2014; Grootemaat et al., 2017 Achchige et al., 2022) the amount of collapsed phloem associated to phloem sap transportation in stress conditions (Gričar & Prislan, 2022), differences of bark thickness due to other triggers (Rocha et al., 2018; Nickolas et al., 2020).

There are reports on the morphological features of eucalyptus (percentage, thickness, and volume) ranging from 10.4% to 42.08% coefficient of variation for bark traits (Wei & Borralho, 1997; Pupin et al., 2017; Câmara et al., 2018). Notwithstanding, bark, and consequently, the secondary phloem, is often discarded and even assumed as an unfavorable trait in the eucalyptus breeding programs (Wei & Boralho, 2000; Pupin et al., 2017; Paludeto et al., 2020). To date, these reports also did not access bark histological elements. Considering these sources of variation, a descriptive anatomical and histochemical analysis of selected commercial eucalyptus clones was conducted to support the evaluation and

comprehension of EPD. A quantitative (histometric) analysis will follow based on the promising descriptive data.

The descriptive anatomy of bark samples from commercial *E. grandis*, *E. urophylla* and *E. grandis* x *E. urophylla* hybrid clones was approached covering features from cambium to periderm cells. Adaptations in the protocol, such as ethanol fixation and extended period of the samples in resin solution under vacuum at 8ºC, allowed adequate processing of eucalyptus bark samples suitable for anatomical studies. Different sectioning planes and maintaining a fragment of the xylem, contributed to the integrity of cambial initials.

The outer bark of eucalyptus trees is composed of a single to multiple periderms, which contain the phellem, phellogen, phelloderm, and secondary phloem. These tissues that are eliminated with the recurrent formation of new phellogen. Although descriptive studies on bark contribute to eucalyptus identification (Quilhó et al., 1999; Jorge et al., 2000) and its alternative uses (Miranda et al., 2016), the association of bark anatomy and EPD has not been reported. Bark thickness decreases from bottom up (data not shown) as already reported for eucalypts (Wei & Borralho, 1997; Ridoutt & Sands, 1993; Jorge et al., 2000; Pupin et al., 2017).

The tissue organization in eucalyptus bark was similar among *E. grandis*, *E. urophylla*, and hybrids clones. This similarity holds for samples from genotypes considered more or less resistant or exhibiting different EPD scores. These findings are consistent across various stem positions evaluated. The observed sequence of tissues consistently included single or multiple periderm (rhytidome), followed by a secondary phloem subdivided into collapsed and non-collapsed portions, and a phloem region characterized by the presence of CaOx crystals. The outer and disorganized parenchyma beneath the periderm seems to derive from axial and radial parenchyma cells. This inference is based on the presence of group of fibers in the outer regions of the same sections and the presence of group of fibers being eliminated with the periderm. This disorganized parenchyma is not continuous along with the periderm. Despite of that, the occurrence of pseudocortex cannot be completely discarded without a follow up of the secondary growth of the eucalyptus stem in addition to this descriptive analysis.

The collapsed and non-collapsed phloem were described for *E. globulus* barks (Quilhó et al., 1999; Jorge et al., 2000), and CaOx are reported in the barks of several eucalyptus species (Lima et al., 2018). On the other hand, differences in the integrity of STE, proportions of secondary phloem with non-collapsed STE and containing CaOx were observed in the samples of the 9 commercial clones evaluated.

Differences in eucalyptus bark thickness (Jordan et al., 2002) and density (Miranda & Pereira, 2015, Almeida et al., 2022) are acknowledged, although EPD tolerant and susceptible eucalyptus clones exhibit similar bark density (Almeida et al., 2022). Nevertheless, in commercial plantations, it was empirically witnessed that barks of EPD susceptible clones are more easily bent compared to EPD tolerant clones, which break when submitted to the same action accompanied by a characteristic noise (data not shown). Hence, differences in eucalyptus barks are thought to be linked with the structure of periderm and phloem tissues in clones diverging their EPD scores. The less organized growth and expansion of axial parenchyma in outer phloem layers along with increased cell collapse observed in EPD are consistent with field observations indicating greater susceptibility or scores above "0".

Jorge et al. (2000) reported a decrease in bark fiber width and wall thickness of *E. globulus* from the base upwards. It was also noted that parenchyma, fibers, rays, sclereids and sieve tubes accounted for 50.0%, 27.9%, 12.1%, 7.3%, and 2.7% of the bark composition, respectively. Nevertheless, cell type proportions varied significantly within the trees. Expanded parenchyma cells (Quilhó et al., 1999) and merging parenchyma rays (Ridoutt & Sands, 1993) have been observed for *E. grandis*, *E. urophylla*, and urograndis hybrids. However, no consistent trend was observed for these traits across studies (Ridoutt & Sands, 1993; Quilhó et al., 1999; Jorge et al., 2000). The expansion of axial parenchyma cells phloem is a common feature of secondary phloem as reported in 11 eucalyptus species (Lima et al., 2018). Considering the difference in cell composition of eucalyptus phloem and bark, it is hypothesized that a less organized phloem and increased proportion of expanded parenchyma cells and collapsed STE could be associated with an increase of EPD symptoms such as bark depressed lesions, cracking and swelling. The observation of an increased proportion of collapsed phloem tissue, or less non-collapsed phloem, in samples with increased EPD scores support this idea.

Rhomboidal calcium oxalate crystals are observed in the axial parenchyma of several eucalyptus species (Lima et al., 2018). These CaOx crystals occur in the non-collapsed phloem and partially overlap with its collapsed counterpart. The extent of these regions varied among the commercial clones, where susceptible clones and clones with EPD symptoms had a smaller proportion of phloem with these inclusions. It is expected that the relative amount of collapsed and non-collapsed phloem, as well as phloem with CaOx crystals, can be associated with EPD intensity or occurrence. CaOx crystals have been reported to serve a surprising function as a dynamic carbon pool. Under drought conditions, they support an "alarm photosynthesis". When the access to atmospheric reserves is limited, the carbon dioxide released from crystal decomposition could be used instead (Tooulakou et al., 2016). Caetano-Madeira et al. (2023) observed that an EPD tolerant eucalyptus had a higher level of calcium in their leaves and attributed it to a better cell structure and homeostasis. Similarly, as CaOx can function as a reduced carbon source (Tooulakou et al., 2016) and as an accessible source of calcium. The calcium content in leaves was selected as one possible biomarker for water deficit (Corrêa et al., 2023) and eucalyptus disorder tolerance (Caetano-Madeira et al., 2023).

Plastids may play a role in the metabolic versatility of eucalyptus clones as proteins and lipids are found in the outer phloem of the evaluated commercial clones. Burrows & Connor (2020) reported the presence of chloroplasts in depths as great as 10 cm of small and larger diameter branches of 23 eucalyptus species. Such chloroplasts occur despite the phellem reducing the light penetration into the stem. The occurrence of these chloroplasts was highlighted as possible trade-offs between photosynthesis and typical functions as protection and mechanical strength, as stem recycling photosynthesis (SRP) could be associated with increased water use efficiency, carbon balance and reducing the effects of drought. Although *E. grandis* and *E. urophylla* were not evaluated in Burrows & Connor (2020) report, the presence of plastids is associated with SRP where chloroplasts refix the CO_2 released by living cells in the bark. EPD tolerant eucalyptus sustained growth could be favored in a similar context as these plastids could contribute to carbon fixation and the instantaneous water use efficiency under stress. Accordingly, the susceptible clone

exhibited a higher photosynthetic rate and reduced dry biomass accumulation, implying less efficient carbon use (Caetano-Madeira et al., 2023).

The observation of preserved plastids with protein inclusions might have been favored by the ethyl alcohol fixation precipitating proteins (Huang & Yeung, 2015). The proteinaceous phloem-protein observed inside the STE was mostly deposited in a parietal position and associated with the sieve plate. Producing lime plugs upon disturbance to avoid sap and reduce carbon loss (Knoblauch & Oparka, 2012) may be associated with alternative plastid functions. Nascimento et al. (2024) reported significant differences in starch concentration in wood and bark samples of contrasting EPD phenotypes. Although these could not differentiate the tolerant and susceptible clones, the distribution of starch in the xylem and phloem sections were distinctive as it was absent or less available in susceptible clones or in samples of plants with EPD. Significant and negative correlations of starch content in wood samples with the sample EPD score (-0.48) and with the expected phenotype (-0.45) were reported accounting for an association of carbohydrates and EPD (Nascimento et al., 2024). Amyloplasts were observed in phloem and xylem parenchyma cells. S-type plastids and P-type plastids in STEs, as well as protein and lipid-rich plastids in phloem and phelloderm cells were observed. Rosell (2016) suggested that bark thickness has an additional function as carbohydrate storage.

The existence of increased non-collapsed STE and a greater amount of CaOx in EPD-tolerant clones are aligned with the results of the genetic expression studies on eucalyptus with and without EPD symptoms. Rodrigues (2020) reported a total of 2,819 differentially expressed exons (DEG) obtained from plants with and without EPD symptoms. Of these, 1,265 (44.87%) were induced, and 1,554 (55.13%) were repressed in plants with EPD symptoms. It was estimated that 644 genes participate in biological processes, 342 are associated with cellular components, and 890 with molecular function. Among those that exhibited cellular component association, 327 revealed cellular anatomical entities.

Amid the differentially expressed sequences, there were induced genes related to lignin degradation (LAC9 and LAC14) and synthesis (CAD1 and 4-coumarate 3-hydroxylase). Among the repressed genes, one related to gibberellin biosynthesis (GA20OX2) was identified (Rodrigues, 2020). There is evidence for the implication of structural and physiological importance of phloem tissue in EPD tolerance traits. Similarly, there are genes differentially expressed in plants with EPD symptoms, such as Phloem Protein 2-Like A1 (PP2A1) (Rodrigues, 2020). This gene has insecticidal activity and is frequently found binding to other proteins present in the phloem (Dinant et al., 2003; Beneteau et al., 2010). The information on differentially expressed genes (Rodrigues, 2020) and the differences in anatomic structures overlap in an applied genomic approach. There are examples of phenotypic markers useful for early selection of EPD in eucalyptus (Corrêa et al., 2017) and evidence that genomic selection for tree height in *Populus* sp. (Alves et al., 2020). Alves et al. (2020) foresaw that integrating early phenotyping into genomic selection models could increase prediction accuracy and reduce generation intervals in *Populus* breeding programs.

Corymbia ssp from 3 to 4 years of age presented a narrow sense heritability of 0.55 for bark percentage genetic correlations of bark percentage and diameter at breast height over bark (DBHOB) ranging from -0.18 to -0.47 (Paludeto et al., 2020). Increasing stem diameter is expected to occur concomitant with a decrease in bark percentage. However, there is no information on the effect on phloem tissues. Considering the positive relationship between active phloem and EPD tolerance, if phloem functionality is not disclosed, proceeding with this negative selection will result in less adapted plants to abiotic stresses and higher physiological disorders. The pedigree contribution must also be considered as there are differences inherent to species associated with fluctuations in bark %. Bark percentage also tends to decrease with age (Sartori et al., 2016; Lima et al., 2018; Paludeto et al., 2020) and increase with stem diameter (Wei & Borralho, 1997; Pupin et al., 2017). Increased tree mortality with age (Mueller-Dombois, 1986; Floyd et al., 2009) and the importance of phloem tissues are necessary to plant resilience under stress (Rosell, 2016), highlight that decreasing bark percentage, disregarding phloem tissue, may be detrimental to the selection of future eucalyptus commercial clones.

Nickolas et al. (2020) observed significant variation in wood basic density estimated by traditional and resistance drilling (RESI)-derived (non-destructive) methods. RESI trace initiates and terminates at the outer bark, with changes in resistance occurring at the bark/wood boundaries, which allows quantifying bark thickness in different positions simultaneously (Downes et al., 2018). This approach could be useful to support empirical and histological observations of eucalyptus bark associated with EPD tolerance, such as bark thickness being positively associated with site temperature annual range and seasonality (Nickolas et al., 2020). A non-significant correlation between bark thickness and wood density and independent results from DBH (Nickolas et al., 2020) supports that bark and phloem traits may be identified and selected without jeopardizing wood quality traits. Bark thickness was already correlated with functional traits of adaptative significance (Jordan et al., 2002; Rosell, 2016).

The importance of histological analysis in understanding the complex relationship between back characteristics and wood properties cannot be overstated. Reports on leaf histometry indicate that vascular tissue, phloem included, is associated with water deficit tolerance (Condé et al., 2020a), as well as EPD tolerance in eucalyptus (Condé et al., 2020b). STE may undergo diverse differentiation depending on environmental triggers. The elements produced in the fall are narrower and have a higher resistance to flow than the ones produced in spring (Prislan et al., 2013). This also applies to bark samples, as physiological and anatomical changes in the phloem correlated with the winter season, may impose physical limits to carbon, nutrient, and signal transportation (Ray & Savage, 2021).

There are cytological, anatomical, and histological elements described in the present report that are useful for characterization and applied purposes. The easily observed P-type plastid, differences in live, non-collapsed, and phloem with CaOx crystals are evidenced. There are differences in the proportion of phloem elements that need a histometric approach allowing their measurement and further association with growth and EPD resistance. These allometric differences may represent trends towards an ideotype based on the qualitative anatomical traits, aiding in the differentiation of commercial eucalyptus clones that are more and less tolerant to EPD.

Conclusions

The organization and structure of bark and secondary phloem is consistent among contrasting EPD clones and trees with different EPD scores. However, analysis of eucalyptus clones revealed distinct proportions of non-collapsed/collapsed sieve tube elements and the presence of CaOx crystals. These findings suggest a relation between bark anatomical and the occurrence as well as tolerance to EPD. Specifically, the proportion of the secondary phloem CaOx crystals, along with the length of live and non-collapsed phloem emerge as potential biomarkers for EPD tolerance.

Funding

This experiment was part of a collaborative research and induced demand project with the financial support of Suzano S/A (Contract number 86/2020). The project also received grants and funding from the Foundation for Research Support of the State of Minas Gerais (FAPEMIG) (Project/process number APQ 01270 13). This study was financed in part by the Coordenação de Aperfeiçoamento de Pessoal de Nível Superior—Brasil (CAPES)—Finance Code 001. This study was financed in part by the National Council for Scientific and Technological Development – CNPq. This study was financed in part by the National Council for Scientific and Technological Development – CNPq.

Acknowledgements

The company Suzano S/A, for the provision of clones to carry out experiments and permission to publish the results. To Alaina Anne Kleine for reviewing the manuscript.

References

ABARES, Australian Bureau of Agricultural and Resource Economics and Sciences. (2019): Australian forest profiles: Eucalypt, Australian Bureau of Agricultural and Resource Economics and Sciences, Canberra, https://doi.org/10.25814/5d9167d34241f. https://www.agriculture.gov.au/sites/default/files/abares/forestsaustralia/publishingimages/forest%20profiles%202019/eucalypt/AusForProf_2019_Eucalypt_v.1.0.0.pdf Accessed in 20 April, 2024.

Alfenas, A. C., Zauza, E. A. V., Mafia, R.G., de Assis, T. F. (2009): Clonagem e Doenças do Eucalipto. 2ª Edition, UFV Press, Viçosa, 500p

Almeida, M. N. F., Picoli, E. A. T., Moulin, J. C., Guimarães, L. M. S., Zauza, E. A. V., Loos, R. A., Hall, K. B., Gomes, D. S., Conceição, G. J., Rodrigues, P. D., Vidaurre, G. B. (2020): Propriedades da madeira como potenciais biomarcadores de tolerância a distúrbios fisiológicos: comparação de genótipos de eucalipto divergentes. Scientia Forestalis, 50: e3864. https://doi.org/10.18671/scifor.v50.22

Alves, F.C., Balmant, K.M., Resende Jr, M.F.R., Kirst, M., de los Campos, G. (2020): Accelerating Forest tree breeding by integrating genomic selection and greenhouse phenotyping. The Plant Genome. 13(3): e20048. https://doi.org/10.1002/tpg2.20048

Andrade Bueno, I. G., Picoli, E. A. T., dos Santos Isaias, R. M., Lopes-Mattos, K. L. B., Cruz, C. D., Kuki, K. N., Zauza, E. A. V. (2020): Wood anatomy of field grown eucalypt genotypes exhibiting differential dieback and water deficit tolerance. Current Plant. 22: 100136. https://doi.org/10.1016/j.cpb.2020.100136

Angyalossy, V., Pace, M. R., Evert, R.F., Marcati, C. R., Oskolski, A.A., Terrazas, T., Kotina, E., Lens, F., Mazzoni-Viveiros, S. C., Angeles, G., Machado, S. R., Crivellaro, A., Rao, K. S., Junikka, L., Nikolaeva, N., Baas, P. (2016): IAWA List of Microscopic Bark Features. IAWA Journal. 37(4): 517-615. https://doi.org/10.1163/22941932-20160151

Beneteau, J., Renard, D., Marché, L., Douville, E., Lavenant, L., Rahbé, Y., Dupont, D., Vilaine, F., Dinant, S. (2010): Binding properties of the N-acetylglucosamine and high-mannose N-glycan PP2-A1 phloem lectin in *Arabidopsis*. Plant Physiology. 153(3): 1345-1361. https://doi.org/10.1104/pp.110.153882

Brando, P. M., Nepstad, D. C., Balch, J. K., Bolker, B., Christman, M. C., Coe, M., Putz, F. E. (2012): Fire-induced tree mortality in a neotropical forest: the roles of bark traits, tree size, wood density and fire behavior. Global Change Biology. 18: 630-641. https://doi.org/10.1111/j.1365-2486.2011.02533.x

Burrows, G. E. Connor, C. (2020): Chloroplast Distribution in the Stems of 23 Eucalypt Species. Plants. 9(12): 1814. https://doi.org/10.3390/plants9121814

Caetano-Madeira, D. D., Omena-Garcia, R. P., Elerati, T.L., da Silva Lopes, C. B., Corrêa, T. R., de Souza, G. A., Oliveira, L. A., Cruz, C.D., Bhering, L. L., Nunes-Nesi, A., Costa, W. G., Picoli, E. A. T. (2023): Metabolic, Nutritional and Morphophysiological Behavior of Eucalypt Genotypes Differing in Dieback Resistance in Field When Submitted to PEG-Induced Water Deficit. Agronomy. 13(5): 1261. https://doi.org/10.3390/agronomy13051261

Câmara, A. P., Oliveira, J. T. S., Bobadilha, G. S., Vidaurre, G. B., Tomazello Filho, M., Soliman, E. P. (2018): Physiological disorders affecting dendrometric parameters and Eucalyptus wood quality for pulping wood. Cerne. 24(1): 27-34. https://doi.org/10.1590/01047760201824012480

Cernusak, L. A., Cheesman, A. W. (2015): The benefits of recycling: How photosynthetic bark can increase drought tolerance. New Phytologist. 208: 995–997. https://doi.org/10.1111/nph.13723

Ciesla, W. M., Donaubauer, M. E. (1994): Decline and Dieback of Trees and Forests: A Global Overview. FAO Forestry Paper, n. 120. FAO, Rome.

Condé, S. A., Picoli, E. A. T., Corrêa, T. R., dos Santos Dias, L. A., Lourenço, R. D. S., dos Santos Silva, F. C., Pereira, W. L., Zauza, E. A. V. (2020): Biomarkers for early selection in eucalyptus tolerant to dieback associated with water deficit. Revista Brasileira de Ciências Agrárias. 15(3): e7515. https://doi.org/10.5039/agraria.v15i3a7515

Condé, S. A., Picoli, E. A. T., Corrêa, T. R., Lourenço, R. D. S. (2020): Marcadores anatômicos do pecíolo e a tolerância à seca de ponteiros e ao déficit hídrico em eucalipto. Nativa. 8(4): 591-596. https://doi.org/10.31413/nativa.v8i4.8702

Corrêa, T. R., Picoli, E. A. T., Pereira, W. L., Condé, A. S., Resende, R. T., de Resende, M. D. V., da Costa, W. G., Cruz, C. D., Zauza, E. A. V. (2023): Very early biomarkers screening for water deficit tolerance in commercial *Eucalyptus* clones. Agronomy. 13(3): 937. https://doi.org/10.3390/agronomy13030937

Corrêa, T. R., Picoli, E. A. T., Souza, G. A., Condé, S. A., Silva, N. M., Lopes-Matos, K. L., Resende, M.D.V., Zauza, E.A.V., Oda, S. (2017): Phenotypic markers in early selection for tolerance to dieback in *Eucalyptus*. Industrial Crops and Products. 107: 130–138. http://dx.doi.org/10.1016/j.indcrop.2017.05.032

Dias, C. N., Picoli, E. A. T., Souza, G. A., Farag, M. A., Scotti, M. T., Barbosa Filho, J. M., da Silva, M. S., Tavares, J. F. (2017): Phenolics metabolismo provides a tool for screening drought tolerant *Eucalyptus grandis* hybrids. Australian Journal of Crop Science. 11(8): 1016–1025. https://doi.org/10.21475/ajcs.17.11.08.pne511

Dinant, S., Clark, A. M., Zhu, Y., Vilaine, F., Palauqui, J.-C., Kusiak, C., Thompson, G. A. (2003): Diversity of the Superfamily of Phloem Lectins (Phloem Protein 2) in Angiosperms, Plant Physiology. 131(1): 114–128. https://doi.org/10.1104/pp.013086.

Downes, G. M., Lausberg, M., Potts, B., Pilbeam, D., Bird, M., Bradshaw, B. (2018): Application of the IML Resistograph to the infield assessment of basic density in plantation eucalypts. Australian Forestry. 81(3): 177–185. https://doi.org/10.1080/00049158.2018.1500676

Dutkowski G. W., Potts B. M. (1999): Geographic Patterns of Genetic Variation in *Eucalyptus globulus* ssp. *globulus* and a Revised Racial Classification. Australian Journal of Botany. 47: 237-263. https://doi.org/10.1071/BT97114

Fensham, R. J., Holman, J. E. (1999): Temporal and spatial patterns in drought-related tree dieback in Australian savanna. Journal of Applied Ecology. 36 1035–1050.

Ferreira, F. A. (1989): *Patologia florestal, Principais doenças florestais no Brasil*. Viçosa, Sociedade de Investigações Florestais. Brasil, 570.

Floyd, M. L., Clifford, M., Cobb, N. S., Hanna, D., Delph, R., Ford, P., Turner, D. (2009): Relationship of stand characteristics to drought-induced mortality in three Southwestern piñon–juniper woodlands. Ecological Applications, 19(5), 1223–1230. https://doi.org/10.1890/08-1265.1

Foelkel, C. E. B. (2005): Casca da árvore do eucalipto: aspectos morfológicos, fisiológicos, florestais, ecológicos e industriais, visando a produção de celulose e papel. In: Foelkel CEB, editor. Eucalyptus OnLine Book & Newsletter [online]: 13–63. Available at: http://www.eucalyptus.com.br/capitulos/capitulo_casca.pdf [accessed 06 February 2023].

Gričar, J., Prislan, P. (2022): Seasonal changes in the width and structure of non-collapsed phloem affect the assessment of its potential conducting efficiency. IAWA Journal, 43(3): 219-233. https://doi.org/10.1163/22941932-bja10084

Grootemaat, S., Wright, I., Bodegom, P., Cornelissen, J., Shaw, V. (2017): Bark traits, decomposition and flammability of Australian forest trees. Australian Journal of Botany. 65(4): 327-338. https://doi.org/10.1071/BT16258

Hua, L. S., Chen, L.W., Antov, P., Kristak, L., Tahir, P. M. (2022): Engineering Wood Products from *Eucalyptus* spp. Adv. Mater. Sci. Eng., 1: 8000780. https://doi.org/10.1155/2022/8000780

Huang, B. Q., Yeung, E. C. (2015): Chemical and Physical Fixation of Cells and Tissues: An Overview In: E. C. T. Yeung et al. (eds.), Plant Microtechniques and Protocols, Springer International Publishing Switzerland. 23-43.

Indústria Brasileira ee Árvores. Relatório Anual IBÁ 2023. (2023): Available at: < https://iba.org/datafiles/publicacoes/relatorios/relatorio-anual-iba2023-r.pdf>. Accessed in, December, 28, 2023.

Jensen, W. A. (1962): Botanical histochemistry: principles and practice. 1st ed., Berkley: W. H. Freeman & Co, 408p.

Johansen, D. A. (1940): Plant microtechnique. New York: McGraw-Hill. 523 p.

Jordan, G. J., Potts, B.M., Clarke, A. (2002): Susceptibility of *Eucalyptus globulus* ssp. *globulus* to sawfly (*Perga affinis* ssp. *insularis*) attack and its potential impact on plantation productivity. Forest Ecology and Management. 160(1): 189–199. https://doi.org/10.1016/S0378-1127(01)00445-5

Jorge, F., Quilhó, T., Pereira, H. (2000): Variability of fiber length in wood and bark in *Eucalyptus globulus.* IAWA Journal. 21(1): 41–48. https://doi.org/10.1163/22941932-90000235

Knoblauch, M., Oparka, K. (2012): The structure of the phloem--still more questions than answers. Plant Journal. 70(1): 147-56. https://doi.org/10.1111/j.1365-313X.2012.04931.x

Landsberg, J. (1985): Drought and dieback of rural eucalypts. Australian Journal of Ecology. 10: 87–90. https://doi.org/10.1111/j.1442-9993.1985.tb00868.x

Lima, L., Miranda, I., Knapic, S., Quilhó, T., Pereira, H. (2018): Chemical and Anatomical Characterization, and Antioxidant Properties of Barks from 11 *Eucalyptus* Species. European Journal of Wood and Wood Products. 76: 783–792. https://doi.org/10.1007/s00107-017-1247-y

Lison, L. A. (1960): Histochemie et cytochemie animales: principles et méthodes. Paris: Gaulthier Villars. 606p.

Matusick, G., Ruthrof, K. X., Hardy, G. S. J. (2012): Drought and heat triggers sudden and severe dieback in a dominant mediterranean-type woodland species. Open Journal of Forestry. 2(4): 183-186. https://doi.org/10.4236/ojf.2012.24022

Miranda, I., Lima, L., Quilhó, T., Knapic, S., Pereira, H. (2016): The bark of *Eucalyptus sideroxylon* as a source of phenolic extracts with anti-oxidant properties. Industrial Crops and Products. 82: 81–87. https://doi.org/10.1016/j.indcrop.2015.12.003

Miranda, I., Pereira, H. (2015): Variation of wood and bark density and production in coppiced *Eucalyptus globulus* trees in a second rotation. iForest, 9(2): 270-275. https://doi.org/10.3832/ifor1442-008

Moulin, J. C., de Souza Ribeiro, D., Vidaurre, G.B., Braga Mulin, L., Moreira, S. I. (2022): Effect of drought stress on the formation and lignification of eucalyptus wood cells. IAWA Journal. 43(3): 263-275. https://doi.org/10.1163/22941932-bja10092

Mueller-Dombois, D. (1986): Perspectives for an etiology of stand-level dieback. Annual Review of Ecology, Evolution, and Systematics. 17: 221–243. https://doi.org/10.1146/annurev.es.17.110186.001253

Nascimento, D. L., Aguiar, V.P., Jacomini, F. A., Costa, E. G., Ribeiro, W. S., Domokos-Szabolcsy, E., Kleine, A. A., Balmant, K. M., Picoli, E. A. T., Zauza, E. A. V., Guimarães, L. M. S. (2024): Rapid detection of bromatological and chemical biomarkers of clones tolerant to eucalyptus physiological disorder. South African Journal of Botany. 175: 684-695. https://doi.org/10.1016/j.sajb.2024.10.052

Nickolas, H., Williams, D., Downes, G., Harrison, P.A., Vaillancourt, R. E., Potts, B. M. (2020): Application of resistance drilling to genetic studies of growth, wood basic density and bark thickness in *Eucalyptus globulus*. Australian Forestry. 83(3): 172-179. https://doi.org/10.1080/00049158.2020.1808276

O'Brien, T. P., Feder, N., McCully, M. E. (1964): Polychromatic staining of plant cell walls by toluidine blue O. Protoplasma 59(2): 368-373. https://doi.org/10.1007/BF01248568

Paludeto, J. G. Z., Bush, D., Estopa, R. A., Tambarussi, E. V. (2020): Genetic control of diameter and bark percentage in spotted gum (*Corymbia* spp.): can we breed eucalypts with more wood and less bark? Southern Forests. 82(1): 86-93. https://doi.org/10.2989/20702620.2020.1733771

Picoli, E. A. T., de Resende, M. D. V., Oda, S. (2021): Come Hell or High Water: Breeding the Profile of Eucalyptus Tolerance to Abiotic Stress Focusing Water Deficit. In: Gupta, D.K., Palma, J.M. (eds) Plant Growth and Stress Physiology. Plant in Challenging Environments. Vol 3. Springer, Cham. 91-127. https://doi.org/10.1007/978-3-030-78420-1_5

Pupin, S., Zaruma, D.U.G., de Souza, C. S., Cambuim, J., Coleto, A. L., Alves, P. F., Pavan, B. E., de Moraes, M. L. T. (2017): Genetic parameters for growth traits, bark thickness and basic density of wood in progenies of *Eucalyptus urophylla* S.T. Blake. Scientia Forestalis. 45(115): 455-465. https://doi.org/dx.doi.org/10.18671/scifor.v45n115.04

Quilhó, T., Pereira, H., Richter, H. G. (1999): Variability of bark structure in plantation-grown *Eucalyptus globulus*. IAWA Journal. 20(2): 171-180. https://doi.org/10.1163/22941932-90000677

Ramirez, M., Rodriguez, J., Balocchi, C., Peredo, M., Elissetche, J. P., Mendonca, R., Valenzuela, S. (2009): Chemical composition and wood anatomy of *Eucalyptus globulus* clones: variations and relationships with pulpability and hand sheet properties. Journal of Wood Chemistry and Technology. 29: 43–58. https://doi.org/10.1080/02773810802607559

Ray, D. M., Savage, J. A. (2021): Seasonal changes in temperate woody plant phloem anatomy and physiology: implications for long-distance transport. AoB Plants. 13(4): plab028. https://doi.org/10.1093/aobpla/plab028

Ridoutt, B. G., Sands, R. (1993): Within-tree variation in cambial anatomy and xylem cell differentiation in *Eucalyptus globulus*. Trees. 8: 18–22. https://doi.org/10.1007/BF00240977

Rodrigues, A. C. P. (2020): Perfil de expressão gênica em híbridos de *Eucalyptus grandis* x *Eucalyptus urophylla* afetados pelo distúrbio fisiológico do eucalipto (DFE), PhD Thesis, Universidade Federal dos Vales do Jequitinhonha e Mucuri, Diamantina, MG, Brazil.

Rodrigues, B. P., da Silva Oliveira, J. T., Demuner, B. J., Mafia, R. G., Vidaurre, G. B. (2022): Chemical and Kraft Pulping Properties of Young Eucalypt Trees Affected by Physiological Disorders. Forests. 13(4): 504. https://doi.org/10.3390/f13040504

Rosell, J. A. (2016): Bark thickness across the angiosperms: more than just fire. New Phytologist. 211(1): 90–102. https://doi.org/10.1111/nph.13889

Sartori, C., Mota, G. S., Ferreira, J., Miranda, I., Mori, F. A., Pereira, H. (2016): Chemical characterization of the bark of *Eucalyptus urophylla* hybrids in view of their valorization in biorefineries. Holzforschung. 70: 1–10. https://doi.org/10.1515/hf-2015-0258

Stanturf, J. A., Vance, E. D., Fox, T. R., Kirst, M. (2013): *Eucalyptus* beyond its native range: environmental issues in exotic bioenergy plantations. International Journal of Forestry Research. 2013(1): 463030. https://doi.org/10.1155/2013/463030

Subasinghe, Y., Volkova, L., Filkov, A., Weston, C. (2022): Effect of bark properties on the cambium cell viability of Eucalyptus species under low radiative heat exposure. Forest Ecology Management. 521: 120443. https://doi.org/10.1016/j.foreco.2022.120443

Tooulakou, G., Giannopoulos, A., Nikolopoulos, D., Bresta, P., Dotsika, E., Orkoula, M. G., Kontoyannis, C. G., Fasseas, C., Liakopoulos, G., Klapa, M. I., Karabourniotis G. (2016): Reevaluation of the plant "gemstones": Calcium oxalate crystals sustain photosynthesis under drought conditions. Plant Signaling & Behavior, 11(9): e1215793 https://doi.org/10.1080/15592324.2016.1215793

Vidal, B. D. C. (1977): Acid glycosaminoglycans and endochondral ossification: microspectrophotometric evaluation and macromolecular orientation. Cellular and Molecular Biology. 22(1): 45-64.

Vieira Rocha, M. F., Pereira, B., Oliveira, A., Pego, M., Veiga, T., Carneiro, A. (2018): Influence of plant spacing on the bark properties of a eucalyptus clone. Rev. Árv., 42(5): e420501. https://doi.org/10.1590/1806-90882018000500001

Walden, L. L., Fontaine, J. B., Ruthrof, K. X., Matusick, J., Harper, R. J., Hardy, G. E. S. J. (2019): Carbon consequences of drought differ in forests that resprout. Global Change Biology. 25(5): 1653-1664. https://doi.org/10.1111/gcb.14589

Wei, X., Borralho, N. M. G. (1997): Genetic control of wood basic density and bark thickness and their relationships with growth traits of *Eucalyptus urophylla* in south east China. Silvae Genetica. 46(4): 245- 250.

Wei, X., Borralho, N. M. G. (2000): Genetic gains and levels of relatedness from best linear unbiased prediction selection of *Eucalyptus urophylla* for pulp production in southeastern China. Canadian Journal of Forest Research. 30: 1601–1607. https://doi.org/10.1139/x00-092

Wesolowski, A., Adams, M., Pfautsch, S. (2014): Insulation capacity of three bark types of temperate Eucalyptus species. Forest Ecology and Management. 313: 224–232. https://doi.org/10.1016/j.foreco.2013.11.015